1992

Dynamics of an Orbiting Scroll with Axial Compliance, Part I - Simulation of Orbiter Axial Motion

H. T. Shu
United Technologies Research Center

A. A. Peracchio
United Technologies Research Center

DYNAMICS OF AN ORBITING SCROLL WITH AXIAL COMPLIANCE
PART 1 - SIMULATION OF ORBITER AXIAL MOTION

H.T. Shu and A.A. Peracchio
United Technologies Research Center
Silver Lane · M.S. 19
East Hartford, CT 06108

ABSTRACT

A dynamic model was developed for investigating the axial motion of an orbiting scroll design which incorporates passive axial and radial compliance mechanisms. The model uses three degrees of freedom to describe the orbiting scroll axial motion. It also includes contact constraints for the thrust surface, the wrap tip and flanks, the crank case, and the hub bearing. The equations of motion were derived using the Lagrangian formulation. The system natural frequencies were predicted, and forced response analyses were performed. Results of the orbiting scroll dynamics analysis not only show good agreement with the experimental data, but also highlight the importance of the constraints.

1. INTRODUCTION

A comprehensive research program has been undertaken by the United Technologies Research Center (UTRC) to develop improved understanding of scroll compressor performance and dynamics in support of Carrier's product applications. This research program consists of not only extensive analytical modeling but also experimental investigation of system performance, pressures, temperatures, vibrations, and dynamic characteristics using instrumented compressors (Ref. 1). In this paper, a simulation of the orbiting scroll axial motion is presented.

Several investigations of scroll compressor dynamic behavior involving orbiter motion have been reported (Refs. 2 to 4). These studies (which usually include an orbiter, an Oldham coupling ring, an axial and radial compliance mechanism, and a crank shaft) have been developed using D'Alembert's principle to model the orbiter inertial effects. These studies assumed that the orbiter motion was constrainted to be in a plane perpendicular to the shaft centerline and within that plane, to execute a circular orbiting motion. Some have allowed for variations in shaft speed (Ref.3). The effect of damping and stiffness of the backchamber seal mechanism on the axial motion were not considered These studies have served as first generation scroll compressor design tools. However, in order to further improve understanding of compression efficiency, component reliability and compressor noise, the development of a more sophisticated dynamic model is required to account for additional degrees of freedom of motion and backchamber seal effects.

2. DYNAMIC MODELING

The dynamic model developed for investigating the scroll orbiter axial motion is described in this section. The model consists of three degrees of freedom represented by three generalized coordinates. It also accounts for motion constraints that might occur due to wrap tip contact with the mating baseplate, wrap flank contact with that of the fixed scroll at other than the ideal contact line, the thrust surface contact, motion constrained by the mechanical limits of the compression of the backchamber seals, and finally, contact of the orbiter hub with the drive shaft mechanism.

2.1 Equations of Motion

The schematic diagram of an orbiting scroll model is shown in Fig. 1, where F_z, M_x, and M_y represent the axial component of the time varying load and the x and y components of the time varying moments acting on the orbiter during comperssor operations. (Further descriptions of these three parameters will be given in the Case-Study Section.) The orbiter is supported by two or three backchamber seals with radii r_1, r_2, and r_3 respectively.

Let 1) (X_f, Y_f, Z_f) be the inertial coordinate system with origin O_f fixed at the shaft center, 2) (x, y, z) be the moving coordinate system with origin O_o fixed at the center of the baseplate bottom surface of orbiting scroll and always parallel to the inertial coordinate system throughout the entire compressor operation, 3) (r_o, Ω) be the radius of orbiting circle and shaft speed, and 4) $(z_o, \theta_x, \theta_z)$ be the generalized coordinates describing the orbiter axial translation and rotations of x and y axes. If z_o, θ_x, and θ_y are small, the displacement and velocity vectors of a small element of the orbiter at point $P(x, y, z)$ can be

expressed in terms of these parameters as follows.

$$\vec{u}_p = [-(r_o sin\ \Omega t)\Omega dt + z\theta_y]\ \vec{i} + [(r_o cos\ \Omega t)\Omega dt - z\theta_x]\ \vec{j} + [y\ \theta_x - x\ \theta_y + z_o]\ \vec{k} \quad (1)$$

$$\dot{\vec{u}}_p = [-\Omega r_o sin\ \Omega t + z\dot{\theta}_y]\ \vec{i} + [\Omega r_o cos\ \Omega t - z\dot{\theta}_x]\ j + [y\ \dot{\theta}_x \quad x\ \dot{\theta}_y + \dot{z}_o]\ \vec{k} \quad (2)$$

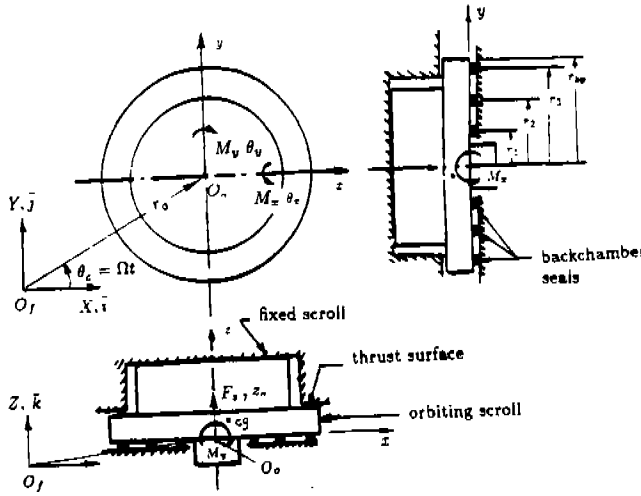

Fig. 1 Schematic Diagram of Orbiting Scroll Dynamics Model

The system kinetic energy (T) and potential energy (V) can be approximated by the following two equations.

$$\begin{aligned} T &= \frac{1}{2}\int_V \dot{\vec{u}}_p \cdot \dot{\vec{u}}_p\ dm \\ &= \frac{1}{2}r_o^2\Omega^2 m + \frac{1}{2}m\dot{z}_o^2 + \frac{1}{2}I_{xx}\dot{\theta}_x^2 + \frac{1}{2}I_{yy}\theta_y^2 - I_{xy}\dot{\theta}_x\dot{\theta}_y + e_{cy}m\dot{z}_o\dot{\theta}_x - e_{cx}m\dot{z}_o\dot{\theta}_y \\ &\quad -(e_{cx}m\Omega r_o cos\ \Omega t)\dot{\theta}_x - (e_{cx}m\Omega r_o sin\ \Omega t)\dot{\theta}_y \end{aligned} \quad (3)$$

$$\begin{aligned} V &= \sum_i V_i \equiv \sum_i \frac{1}{2}\int_0^{2\pi} [(\vec{u}_p \cdot \vec{k})^2]_i\ k_i\ r_i\ d\phi \\ &= \sum_i [\pi k_i r_i z_o^2 + \frac{\pi}{2}k_i r_i^3(\theta_x^2 + \theta_y^2)] \end{aligned} \quad (4)$$

where $m, e_{cx}, e_{cy}, I_{xx}, I_{yy}, I_{xy}$ are the orbiter mass, center of gravity, and moments and products of inertia, and $k_i, i = 1,2,3$, are the backchamber seal stiffnesses per unit length.

The system generalized forces Q_i can be derived in terms of the axial load, F_z, moments, M_x and M_y, body force, mg_c, and seal damping values, $c_i, i = 1,2,3$, using the following virtual work concept.

$$\begin{aligned} \delta W &= Q_1\ \delta z_o + Q_2\ \delta\theta_x + Q_3\ \delta\theta_y \\ &= (F_z - mg_c)\delta z_o + (M_x - mg_c e_{cy})\ \delta\theta_x + (M_y + mg_c e_{cx})\ \delta\theta_y - \\ &\quad \int_0^{2\pi}(\textstyle\sum_i c_i r_i d\phi)(\dot{u}_p \delta u_p)_{z=0} \end{aligned}$$

$$= (F_z - mg_c - 2\pi \sum_i c_i r_i \dot{z}_o)\delta\dot{z}_o + (M_x - mg_c e_{cy} - \pi \sum_i c_i r_i^3 \dot{\theta}_x)\delta\theta_x + (M_y + mg_c e_{cx} - \pi \sum_i c_i r_i^3 \dot{\theta}_y)\delta\theta_y$$

By comparing the coeffieients of the virtual displacements of the three generalized coordinates, we have

$$Q_i = \{Q\} = \begin{Bmatrix} F_z - mg_c - 2\pi \sum_i c_i r_i \dot{z}_o \\ M_x - mg_c e_{cy} - \pi \sum_i c_i r_i^3 \dot{\theta}_x \\ M_y + mg_c e_{cx} - \pi \sum_i c_i r_i^3 \dot{\theta}_y \end{Bmatrix} \tag{5}$$

Finally, the equations of motion can be derived from the following Lagrange's equation.

$$\frac{d}{dt}\left(\frac{\partial L}{\partial \dot{q}_i}\right) - \frac{\partial L}{\partial q_i} = Q_i \tag{6}$$

where $L = T - V$ and q_i and $\dot{q}_i$ are the generalized coordinates $(z_o, \theta_x, \theta_y)$ and their time derivatives. By carrying out the differentiations of the Lagrange's equation and with the help of Eqs. (3), (4) and (5), we have three equations of motion for the orbiter axial motion, expressed in a matrix form as follows.

$$\begin{bmatrix} m & -e_{cy}m & e_{cx}m \\ -e_{cy}m & I_{xx} & -I_{xy} \\ e_{cx}m & -I_{xy} & I_{yy} \end{bmatrix} \begin{Bmatrix} \ddot{z}_o \\ \ddot{\theta}_x \\ \ddot{\theta}_y \end{Bmatrix} +$$

$$\begin{bmatrix} 2\pi \sum_i c_i r_i & 0 & 0 \\ 0 & \pi \sum_i c_i r_i^3 & 0 \\ 0 & 0 & \pi \sum_i c_i r_i^3 \end{bmatrix} \begin{Bmatrix} \dot{z}_o \\ \dot{\theta}_x \\ \dot{\theta}_y \end{Bmatrix} + \tag{7}$$

$$\begin{bmatrix} 2\pi \sum_i k_i r_i & 0 & 0 \\ 0 & \pi \sum_i k_i r_i^3 & 0 \\ 0 & 0 & \pi \sum_i k_i r_i^3 \end{bmatrix} \begin{Bmatrix} z_o \\ \theta_x \\ \theta_y \end{Bmatrix} = \begin{Bmatrix} F_z \quad mg_c \\ M_x - mg_c e_{cy} - e_{cx} m\Omega^2 r_o sin\Omega t \\ M_y + mg_c e_{cx} + e_{cx} m\Omega^2 r_o cos\Omega t \end{Bmatrix}$$

The orbiting scroll system natural frequencies and mode shapes can be computed using Eq. (7) by dropping both the damping and external load terms. However, because the orbiter is placed in a confined compartment, the forced response dynamics analysis must account for all possible constraints on the orbiter axial motion due to the fixed scroll, Oldham coupling ring, slider block, and crank case. Eight possible motion constraints are depicted in Fig. 2, and are indicated by the $\lambda_i, i = 1, 2, ...8$. It should be noted that λ_1 can occur at the wrap tip of either the orbiting or fixed scroll as shown in Fig. 2 and to be described further in Section 2.3.

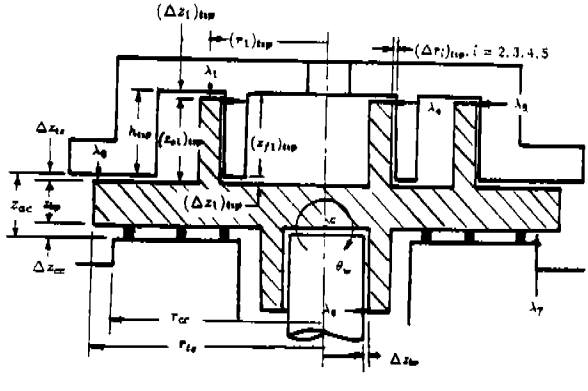

Fig. 2 Constraints of Orbiter Axial Motion

2.2 Equations of Motion Constraints

Figure 3 shows the details of five possible constraint points at the orbiting scroll wrap tips for any given θ_x and θ_y, where the dotted lines represent the wrap profiles of the fixed scroll, the solid lines represent those of the orbiting scroll, point #1 is possible axial contact point, and points #2 to 5 are the possible radial contact points. The geometric locations of these contact points at any given instant (or crank angle) are analytically defined. In other words, the gap between the two scroll wraps for any given θ_x, θ_y are analytically determined. Neglecting the film effects due to orbiter relative motions, the following constraint equations can be easily derived. Fig. 3 illustrates these contact points. Note that the scroll is oriented so that the rotation of the orbiter is along the line A-A.

$$
\begin{aligned}
(\rho_1)_{tip}\cos(\varphi_1 - \theta_w) - (z_1)_{tip} - z_0 &\le (\Delta z_1)_{tip} \quad for\ \lambda_1 \\
(r_2)_{tip} - (\rho_2)_{tip}\sin(\varphi_2 - \theta_w) &\le (\Delta r_2)_{tip} \quad for\ \lambda_2 \\
(r_3)_{tip} - (\rho_3)_{tip}\sin(\varphi_3 - \theta_w) &< (\Delta r_3)_{tip} \quad for\ \lambda_3 \\
(\rho_4)_{tip}\sin(\varphi_4 + \theta_w) - (r_4)_{tip} &\le (\Delta r_4)_{tip} \quad for\ \lambda_4 \\
(\rho_5)_{tip}\sin(\varphi_5 + \theta_w) - (r_5)_{tip} &\le (\Delta r_5)_{tip} \quad for\ \lambda_5
\end{aligned}
\tag{8}
$$

where

$$
\left\{
\begin{array}{l}
(r_i)_{tip} = \sqrt{(x_i^2 + y_i^2)_{tip}} \\
(\rho_i)_{tip} = \sqrt{(x_i^2 + y_i^2 + z_i^2)_{tip}} \\
\varphi_i = \sin^{-1}((r_i)_{tip}/(\rho_i)_{tip})
\end{array}
\right\}, \quad i = 1, \ldots, 5 \tag{9}
$$

$$
\theta_w = \sin^{-1}(-\cos\phi_c \sin\theta_y + \sin\phi_c \sin\theta_x)\,. \tag{10}
$$

$$
\phi_c = \tan^{-1}(-\theta_x/\theta_y) \tag{11}
$$

and $(\Delta z_1)_{tip}$ represents the axial clearance between the tip of the orbiting scroll and the root of the fixed scroll at point #1, and $(\Delta r_2)_{tip}$,..., $(\Delta r_5)_{tip}$ are the radial gaps (or clearances) between points 2 and 2',..., 5 and 5' respectively.

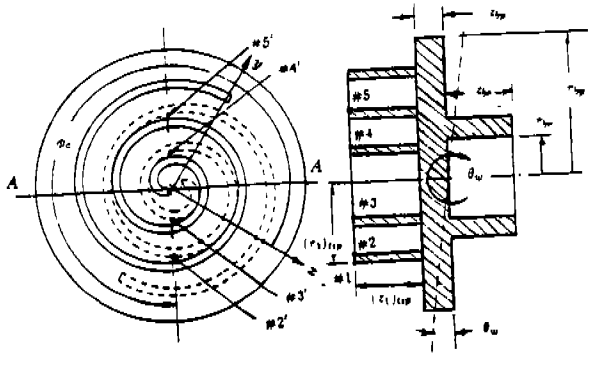

Fig. 3 Configuration of Constraint Models

By refering to Fig. 2, the constraint equations for the thrust surface, hub bearing, and crank case can also be derived as follows.

$$\begin{aligned} \rho_{ts}\, sin(\varphi_{ts} - \theta_w) - z_{bp} - z_o &\le \Delta z_{ts} \quad for\ \lambda_6 \\ z_o + r_{cc}\, sin\, \theta_w &\le \Delta z_{cc} \quad for\ \lambda_7 \\ r_{br} - \rho_{br}\, sin(\varphi_{br} - \theta_w) &\le \Delta r_{br} \quad for\ \lambda_8 \end{aligned} \tag{12}$$

where

$$\begin{aligned} \rho_{ts} &= \sqrt{z_{bp}^2 + r_{bp}^2}, \quad \varphi_{ts} = sin^{-1}(r_{bp}/\rho_{ts}) \\ \rho_{br} &= \sqrt{z_{hb}^2 + r_{br}^2}, \quad \varphi_{br} = sin^{-1}(r_{br}/\rho_{br}) \end{aligned} \tag{13}$$

It should be noted that the eight constraint equations shown in Eqs. (8) and (12) are nonlinear conditional holonomic constraints, and they must be checked at every integration step to see if they are violated. Once one or more constraints are violated, the motion of the orbiter is defined in part by the constraint condition, in which case the equal sign in the appropriate constraint equation defines the relationship that must geometrically exist during the time that the constraint condition is in place. During those time intervals, the constraint equations must be solved with the equations of motion, as described below. It is also important to note that θ_x, θ_y, and θ_w are always small (i.e. less than 0.1 degrees, or 0.002 radians), and Eq. (11) can be approximated by the following relation.

$$\theta_w \simeq (sin\ \phi_c)\, \theta_x - (cos\ \phi_c)\, \theta_y \tag{14}$$

After some mathematical manipulations, the eight constraint equations can be simplified to the following form.

$$\begin{bmatrix} -1 & (r_1)_{tip}\, sin\ \phi_c & -(r_1)_{tip}\, cos\ \phi_c \\ 0 & (z_2)_{tip}\, sin\ \phi_c & -(z_2)_{tip}\, cos\ \phi_c \\ 0 & (z_3)_{tip}\, sin\ \phi_c & -(z_3)_{tip}\, cos\ \phi_c \\ 0 & (z_4)_{tip}\, sin\ \phi_c & -(z_4)_{tip}\, cos\ \phi_c \\ 0 & (z_5)_{tip}\, sin\ \phi_c & -(z_5)_{tip}\, cos\ \phi_c \\ -1 & r_{ts}\, sin\ \phi_c & -r_{ts}\, cos\ \phi_c \\ 1 & r_{cc}\, sin\ \phi_c & -r_{cc}\, cos\ \phi_c \\ 0 & z_{br}\, sin\ \phi_c & -z_{br}\, cos\ \phi_c \end{bmatrix} \begin{Bmatrix} z_o \\ \theta_x \\ \theta_y \end{Bmatrix} \le \begin{Bmatrix} (\Delta z_1)_{tip} \\ (\Delta r_2)_{tip} \\ (\Delta r_3)_{tip} \\ (\Delta r_4)_{tip} \\ (\Delta r_5)_{tip} \\ \Delta z_{ts} \\ \Delta z_{cc} \\ \Delta r_{br} \end{Bmatrix}, \quad or \tag{15}$$

$$a_{jk} q_k \le \Delta b_j, \quad j = 1, ..., 8,\ k = 1, 2, 3$$

2.3 Clearances of Motion Constraints

The instantaneous clearances of the orbiter motion constraints for the right-hand side of Eqs. (15) must be specified. The instantaneous wrap tip clearances, $(\Delta r_2)_{tip}, ..., (\Delta r_5)_{tip}$ can be computed from the geometric locations of the scroll profiles. The hub bearing clearance, Δr_{br}, can be obtained from the design geometry. However, because the heights of the scroll wraps are usually contoured to accommodate the expected thermal expansions, the three axial clearances, $(\Delta z_1)_{tip}$, Δz_{ts}, and Δz_{cc} are related to the wrap heights of the fixed and orbiting scrolls at the contact points and the static axial clearance between the fixed scroll and the crank case, Δz_{ac} as shown in Fig. 2. If finite element structural analysis results are available, the wrap deflection data can also be incorporated into this analysis. Assuming the heights of the fixed and orbiting scroll wraps at the axial contact point are z_{f1} and z_{o1}, the height of the fixed scroll wrap at the thrust surface is h_{tip}, then we have the following relationships.

$$If\ h_{tip} \ge z_{f1}\ and\ h_{tip} \ge z_{o1},\ then \begin{cases} (\Delta z_1)_{tip} = h_{ttp} \quad MAX[(z_{o1})_{tip}, (z_{f1})_{tip}] \\ \Delta z_{ts} = 0 \\ \Delta z_{cc} = z_{ac} - \Delta z_{ts} - z_{bp} \end{cases}$$

$$If\ z_{o1} \ge z_{f1}\ and\ z_{o1} \ge h_{tip},\ then \begin{cases} (\Delta z_1)_{tip} = 0 \\ \Delta z_{ts} = (z_{o1})_{tip} - h_{tip} \\ \Delta z_{cc} = z_{ac} - \Delta z_{ts} - z_{bp} \end{cases} \tag{16}$$

$$If\ z_{f1} \geq z_{o1}\ and\ z_{f1} \geq h_{tip},\ then \begin{cases} (\Delta z_1)_{tip} = 0 \\ \Delta z_{ts} = (z_{f1})_{tip} \quad h_{tip} \\ \Delta z_{cc} = z_{ac} - \Delta z_{ts} - z_{bp} \end{cases}$$

Equation (16) defines which of the axial clearance constraints are activated. It should be noted that the wrap tip and thrust surface constraints can be activated simultaneously or one at a time.

2.4 Equations of Motion with Constraints

It is obvious that if any conditional holonomic constraints are violated, there will be reaction forces exerted on the orbiter at the contact points as shown in Fig. 2. These contact forces can be represented by Lagrange multiplier λ_i. The equations of motion with two constraints, as an example, are given below.

$$\begin{bmatrix} m & -e_{cy}m & e_{cx}m & 0 & 0 \\ -e_{cy}m & I_{xx} & -I_{xy} & 0 & 0 \\ e_{cx}m & -I_{xy} & I_{yy} & 0 & 0 \\ 0 & 0 & 0 & 0 & 0 \\ 0 & 0 & 0 & 0 & 0 \end{bmatrix} \begin{Bmatrix} \ddot{z}_o \\ \ddot{\theta}_x \\ \ddot{\theta}_y \\ 0 \\ 0 \end{Bmatrix} + \begin{bmatrix} 2\pi \sum_i c_i r_i & 0 & 0 & 0 & 0 \\ 0 & \pi \sum_i c_i r_i^3 & 0 & 0 & 0 \\ 0 & 0 & \pi \sum_i c_i r_i^3 & 0 & 0 \\ 0 & 0 & 0 & 0 & 0 \\ 0 & 0 & 0 & 0 & 0 \end{bmatrix} \begin{Bmatrix} \dot{z}_o \\ \dot{\theta}_x \\ \dot{\theta}_y \\ 0 \\ 0 \end{Bmatrix} +$$

$$\begin{bmatrix} 2\pi \sum_i k_i r_i & 0 & 0 & -a_{i1} & -a_{j1} \\ 0 & \pi \sum_i k_i r_i^3 & 0 & -a_{i2} & -a_{j2} \\ 0 & 0 & \pi \sum_i k_i r_i^3 & -a_{i3} & -a_{j3} \\ a_{i1} & a_{i2} & a_{i3} & 0 & 0 \\ a_{j1} & a_{j2} & a_{j3} & 0 & 0 \end{bmatrix} \begin{Bmatrix} z_o \\ \theta_x \\ \theta_y \\ \lambda_i \\ \lambda_j \end{Bmatrix} = \begin{Bmatrix} F_z - mg_c \\ M_x \quad mg_c e_{cy} - e_{cx} m\Omega^2 r_o sin\Omega t \\ M_y + mg_c e_{cx} + e_{cx} m\Omega^2 r_o cos\Omega t \\ \Delta b_i \\ \Delta b_j \end{Bmatrix} \tag{17}$$

where $a_{i1}, a_{i2}, a_{i3}, a_{j1}, a_{j2}, a_{j3}, \Delta b_i$, and Δb_j are the coefficients and constant clearances of the violated i^{th} and j^{th} constraint equations.

3. METHOD OF SOLUTION

Because the coefficients of the equations of motion contain material and inertia properties of the orbiting scroll and backchamber seals, the numerical values of the matrix elements vary greatly in magnitude. To avoid any truncation errors in the numerical integration, all dependent and independent variables are normalized to have numerical values in the order of one. The referenced parameters chosen for this normalization process are

$$\begin{aligned} &z_n = \Delta t^2, \qquad \theta_n = \Delta t^2 / r_{bp}, \qquad I_n = m\, r_{bp}^2, \\ &c_n = m/(\pi\, r_{bp}\, \Delta t), \quad k_n = m/(\pi\, r_{bp}\, \Delta t^2) \end{aligned} \tag{18}$$

where Δt is the integration time step and r_{bp} is the radius of the baseplate. The normalized dependent and independent parameters for the equations of motion and constraints are listed below.

$$\begin{aligned} &\bar{z}_o = z_o/z_n, \qquad \bar{\theta}_x = \theta_x/\theta_n, \qquad \bar{\theta}_y = \theta_y/\theta_n, \\ &\dot{\bar{z}}_o = \dot{z}_o/\Delta t\ z_n, \qquad \dot{\bar{\theta}}_x = \dot{\theta}_x/(\Delta t\ \theta_n), \qquad \dot{\bar{\theta}}_y = \dot{\theta}_y/(\Delta t\ \theta_n), \\ &\ddot{\bar{z}}_o = \ddot{z}_o/(\Delta t^2\ z_n), \qquad \ddot{\bar{\theta}}_x = \ddot{\theta}_x/(\Delta t^2\ \theta_n), \qquad \ddot{\bar{\theta}}_y = \ddot{\theta}_y/(\Delta t^2\ \theta_n), \\ &\bar{r}_i = r_i/r_{bp}, \qquad \bar{c}_i = c_i/c_n, \qquad \bar{k}_i = k_i/k_n, \\ &\bar{I}_{xx} = I_{xx}/I_n, \qquad \bar{I}_{yy} = I_{yy}/I_n, \qquad \bar{I}_{xy} = I_{xy}/I_n, \\ &\bar{e}_{cx} = e_{cx}/r_{bp}, \qquad \bar{e}_{cy} = e_{cy}/r_{bp}, \qquad \bar{e}_{cz} = e_{cz}/r_{bp}, \qquad \bar{r}_o = r_o/r_{bp}, \\ &\bar{t} = t/\Delta t, \qquad \bar{r}_{ts} = r_{ts}/r_{bp}, \qquad \bar{r}_{br} = r_{br}/r_{bp}, \qquad \bar{e}_f = e_f/r_{bp}, \\ &\bar{r}_i = r_i/r_{bp}, \qquad \Delta\bar{z}_i = \Delta z_i/z_n, \qquad \Delta\bar{r}_i = \Delta r_i/z_n, \qquad \bar{F}_z = F_z/m \end{aligned} \tag{19}$$

The normalized equations of motion become

$$\begin{bmatrix} 1 & -\bar{e}_{cy} & \bar{e}_{cx} \\ -\bar{e}_{cy} & \bar{I}_{xx} & -\bar{I}_{xy} \\ \bar{e}_{cx} & -\bar{I}_{xy} & \bar{I}_{yy} \end{bmatrix} \begin{Bmatrix} \ddot{\bar{z}}_o \\ \ddot{\bar{\theta}}_x \\ \ddot{\bar{\theta}}_y \end{Bmatrix} + \begin{bmatrix} 2\sum_i \bar{c}_i \bar{r}_i & 0 & 0 \\ 0 & \sum_i \bar{c}_i \bar{r}_i^3 & 0 \\ 0 & 0 & \sum_i \bar{c}_i \bar{r}_i^3 \end{bmatrix} \begin{Bmatrix} \dot{\bar{z}}_o \\ \dot{\bar{\theta}}_x \\ \dot{\bar{\theta}}_y \end{Bmatrix} +$$

$$\begin{bmatrix} 2\sum_i \bar{k}_i \bar{r}_i & 0 & 0 \\ 0 & \sum_i \bar{k}_i \bar{r}_i^3 & 0 \\ 0 & 0 & \sum_i \bar{k}_i \bar{r}_i^3 \end{bmatrix} \begin{Bmatrix} \bar{z}_o \\ \bar{\theta}_x \\ \bar{\theta}_y \end{Bmatrix} = \begin{Bmatrix} \bar{F}_z - g_c \\ \bar{M}_x - g_c\, \bar{e}_{cy} + \bar{e}_{cz}\Omega^2 \bar{r}_o sin\ \Omega t \\ \bar{M}_y + g_c\, \bar{e}_{cx} + \bar{e}_{cz}\Omega^2 \bar{r}_o cos\ \Omega t \end{Bmatrix} \tag{20}$$

and the normalized constraint equations are

$$\begin{bmatrix} -1 & (\bar{r}_1)_{tip}\ sin\ \phi_c & -(\bar{r}_1)_{tip}\ cos\ \phi_c \\ 0 & (\bar{z}_2)_{tip}\ sin\ \phi_c & -(\bar{z}_2)_{tip}\ cos\ \phi_c \\ 0 & (\bar{z}_3)_{tip}\ sin\ \phi_c & (\bar{z}_3)_{tip}\ cos\ \phi_c \\ 0 & (\bar{z}_4)_{tip}\ sin\ \phi_c & -(\bar{z}_4)_{tip}\ cos\ \phi_c \\ 0 & (\bar{z}_5)_{tip}\ sin\ \phi_c & -(\bar{z}_5)_{tip}\ cos\ \phi_c \\ -1 & \bar{r}_{ts}\ sin\ \phi_c & -\bar{r}_{ts}\ cos\ \phi_c \\ 1 & \bar{r}_{cc}\ sin\ \phi_c & -\bar{r}_{cc}\ cos\ \phi_c \\ 0 & \bar{z}_{br}\ sin\ \phi_c & -\bar{z}_{br}\ cos\ \phi_c \end{bmatrix} \begin{Bmatrix} \bar{z}_o \\ \bar{\theta}_x \\ \bar{\theta}_y \end{Bmatrix} \leq \begin{Bmatrix} (\Delta\bar{r}_1)_{tip} \\ (\Delta\bar{r}_2)_{tip} \\ (\Delta\bar{r}_3)_{tip} \\ (\Delta\bar{r}_4)_{tip} \\ (\Delta\bar{r}_5)_{tip} \\ \Delta\bar{z}_{ts} \\ \Delta\bar{z}_{cc} \\ \Delta\bar{r}_{br} \end{Bmatrix} \tag{21}$$

Because 1) the equations of motion are coupled through the inertia term, 2) the constraint equations are nonlinear and must be checked at every integration step, and 3) the violated constraint equations must be solved simultaneously with the equations of motion, the numerical solution could exhibit stability problems. Therefore the Newmark method was chosen to solve the above dynamics equations because it provides stable numerical solutions to this type of problem.

4. CASE STUDY

The present study is based on design data for an experimental scroll compressor tested in the UTRC compressor laboratory described in a companion paper (Ref. 1).

4.1 Results of Undamped Free Vibration Analysis

The undamped free vibration analysis was performed to identify the system natural frequencies, and the first three harmonic values are 265.68 Hz, 201.04 Hz, and 192.02 Hz respectively. These results indicated that this compressor would not have any resonant problem during steady-state 60 Hz operation.

4.2 Results of Forced Response Analysis

As shown in Eq. (7), the equations of motions require three input forcing functions, $F_z(t), M_x(t)$ and $M_y(t)$. These data were provided by a UTRC quasi-static simulation code. This simulation code is actually the first generation of the UTRC scroll compressor design code, which has been extensively used by Carrier to provide the basic design information for any given scroll compressor capacity and steady-state operating condition. Some of the assumptiuons used in the development of this simulation code are summarized below.

1. The orbiter undergoes a circular orbiting motion around the fixed scroll only in the (X, Y)-plane.
2. The gas pressures surrounding the orbiter are analytically determined at any crank angle for a given steady-state operating condition.
3. The body force and all external loads (including contact forces between the scroll flanks, between the orbiter baseplate and Oldham coupling ring, between the hub bearing and slider block) are in equilibrium with the linear inertia forces in the axial, radial and tangential directions.
4. Summations of all moments in the axial, radial and tangential directions for each hardware component are zero.
5. The inertia effects are considered in every time step, but not carried over to the following step (i.e. quasi-static assumption).

With these assumptions, both the axial component of the reaction force from fixed scroll and the force center required for preventing the orbiter from undergoing axial motion were computed. These data were converted into $F_x(t)$, $M_x(t)$ and $M_y(t)$ for the present study. However, in order to accept the experimental pressure data from any steady-state or transient operations, portions of the original simulation code were modified and integrated with the present model for use in predicting the transient dynamics for any given orbiting scroll design.

A set of the computed and measured pressures for the entire compression process for the same steady-state condition is shown in Fig. 4. Good agreement between the two are indicated. The pressures for all compression pockets and backchamber at any given crank angle, for one revolution, can be easily derived from these data, and results are shown in 5. These data are used for computing the three forcing functions and the results are shown in Fig. 6.

The effects of thermal and pressure loads on the axial growth of orbiting and fixed scroll wraps for various compressor operating conditions are under continuing study. Preliminary results of a finite element structural analysis indicated that the maximum axial growth always occurred at the inner tip of the scroll wrap and the predicted numerical value was approximately 0.0014 in for the test condition (Ref. 5). Based on this preliminary result and the design contours of the two scroll wrap heights, the axial contact constraint point (i.e. corresponding to λ_1 in Fig. 2) would occur near the inner tip of the scroll wrap and cause the orbiter to undergo small wobbles. The predicted orbiting scroll wobble characteristics based on this wrap tip constraint for two high pressure, high load, steady-state operating conditions are shown in Fig. 7a, and those obtained from the experimental study are shown in Fig. 7b. Good agreement between the two is indicated. Both the analytical and experimental results have indicated that the orbiter wobble motions are quite small, and the experimental results showed no impact on the operation of this experimental compressor.

5. CONCLUSIONS

Results of this study indicated that the wrap height contours of both the orbiting and fixed scrolls, which vary with compressor operating conditions, play an important role in the study of orbiter dynamics. The importance of constraints in the dynamic analysis of a given orbiter design is shown. The model presented is capable of predicting the orbiter dynamics of axial motion for steady-state or start-up operation if the wrap heights of both the fixed and orbiting scrolls, the thrust surface, bearing and seal clearences, and the pressure data surrounding the orbiting scroll are prescribed.

6. ACKNOWLEDGEMENT

The authors would like to thank Messrs. D.G. Cutts, R.L. DeBlois, A.J. Marchese, D.J. McFarlin and J.J. Nieter of UTRC and Mr. T. Kassouf of Carrier for their discussions, suggestions and comments during the course of this study.

REFERENCES

1. Marchese, A.J., "Dynamics of An Orbiting Scroll with Axial Compliance, Part - 2 Experimental Techniques", presented at the 1992 Int. Compressor Eng. Conf. at purdue, July 12-14, 1992.

2. Nieter, J.J. and T. Barito, "Dynamics of Compliance Mechanisms in Scroll Compressors, Part I: Axial Compliance" Proceeding of 1990 Int. Compressor Eng. Conf. at Purdue, Vol. 1, pp. 308-316.

3. Ishii, N. et al., "Dynamic Behavior of a Scroll Compressor", JSME International J. Series III, Vol.31, No. 1, 1988.

4. Morishita, E. et al., "Scroll Compressor Dynamics", Bulletin of JSME, Vol. 29, No. 248, Feb. 1986.

5. Marler, M.E. and K.B. Kumar, "Determination of Scroll Wrap Contact Stresses Using the Boundary Element Method", presented at the 1992 Int. Compressor Eng. Conf. at purdue, July 12-14, 1992.

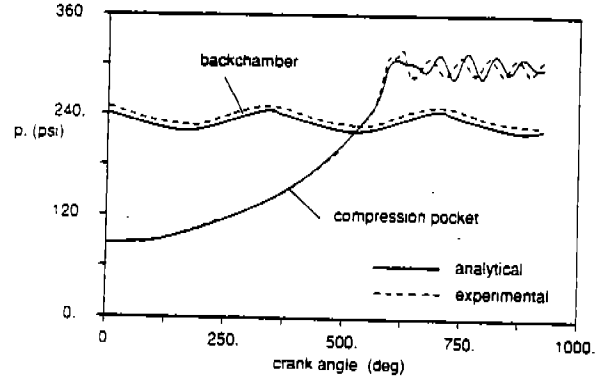

Fig. 4 Comparison of Analytical and Experimental Pressures

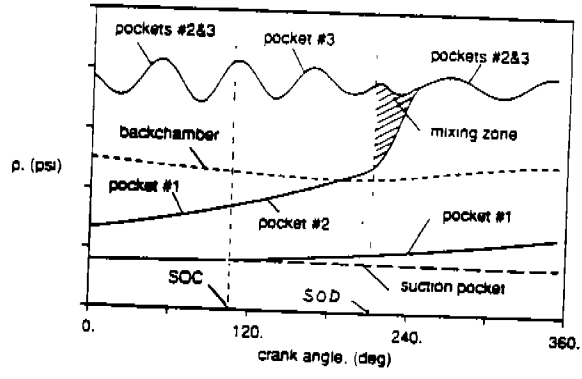

Fig. 5 Gas Pressures for Orbiting Scroll Dynamics Analysis

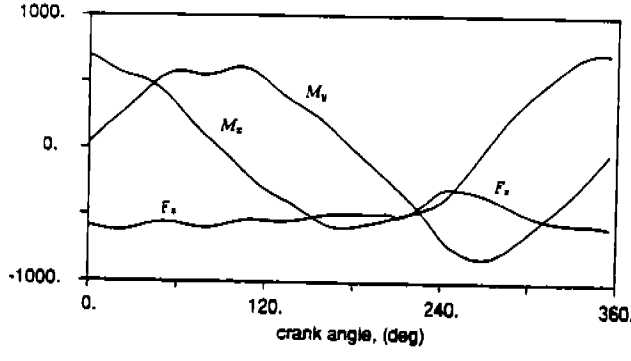

Fig. 6 Forcing Functions for Orbiting Scroll Dynamics Analysis

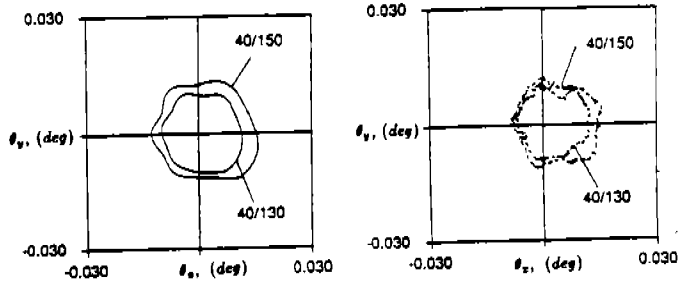

7a) analytical

7b) experimental

Fig. 7 Comparison of Wobble Results